# Evolution of an Intrathermocline Lens over the Lofoten Basin

**Boris N. Filyushkin, Mikhail A. Sokolovskiy and Konstantin V. Lebedev**

## Introduction

Systematic oceanographic surveys conducted by the Arctic and Antarctic Research Institute during the period 1970–1990 in the region of the Lofoten Basin (LB) of the Norwegian Sea proved the existence of a quasistationary anticyclonic vortex (AV) [2]. Six consecutive oceanographic surveys occupied in 1987–1988 have shown the existence of a synoptic-scale (diameter was about 60 km) vortex (a lens) and instrumentally confirmed its anti-cyclonic character. At the same time, during a year, the AV have been drifting almost along a closed cyclonic orbit (with a horizontal latitude scale about 130 km) while its core was still located in the deepest part of the LB (the isobath 3200 m) [6, 7] and Fig. 1 of this contribution.

The development of the Argo project in the first years of the 21st century in addition to the neutral buoyancy floats observations started in the beginning of the 1990s, provides opportunities for studying the structure and circulation of water in the LB. New observations confirmed the existence of a quasi-permanent AV and the fact that the cyclonic circulation dominates in the depth range 600–1000 m within the deepest part of the LB [5, 12, 14, 22]. Detailed measurements performed by the RAFOS floats and Doppler current velocity meters revealed a complex pattern of the formation and existence of a large number of mesoscale vortices that differ in their lifetime and scale. At the same time, the number of vortices in the LB fluctuated throughout the year [19]. Similar results were also obtained from satellite observations of variations in the sea surface height (SSH) and the sea surface temperature [8, 15, 23]. In these publications, satellite images based on weekly

B. N. Filyushkin (✉) · M. A. Sokolovskiy · K. V. Lebedev
Shirshov Institute of Oceanology, Russian Academy of Sciences, Moscow, Russia
e-mail: borisfil@yandex.ru

M. A. Sokolovskiy
Water Problems Institute, Russian Academy of Sciences, Moscow, Russia



M. G. Velarde et al. (eds.), *The Ocean in Motion*, Springer Oceanography,
https://doi.org/10.1007/978-3-319-71934-4_21

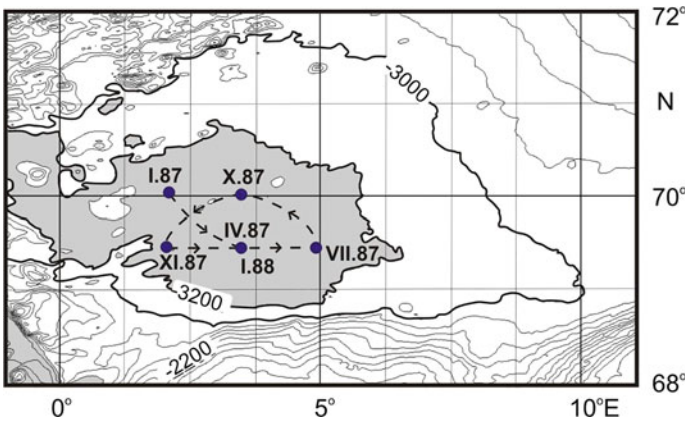


**Fig. 1** Map of the LB bottom topography. The dashed line shows the trajectory of the anticyclonic vortex (lens) and the dots represent the lens location at the times of measurements [7]. The area with the depths deeper than 3200 is shown in gray color

altimeter data have shown the location of mesoscale long-lived vortices of different rotation signs that moved along the cyclonic orbit. At specific stages of the motion, they merged with an anticyclonic vortex located at the center of the deepest part of the LB (3200 m) at 69° 30′ N, 3° E [15]. Currently, the daily data show that the previously recorded long-living vortices represented a cluster of separate short-living eddies, and they better demonstrate the mean eddy drift [16].

The Lofoten Basin is the main reservoir of heat in the Polar seas (PS) [1, 2, 15, 23]. However, the heat content of the central AV is less than the total heat content of the entire LB waters. This means that warm Atlantic waters should submerge [2, 8] in the upper layers in the center of the deepest part of the LB, and at the same time, a deep topographic cyclonic water rotation should exist [5, 14, 15, 22]. In addition, the deepest part of the LB is located between two frontal zones: in the northwest, the front is located along the Mona Ridge, and in the southeast, the front is represented by the Norwegian Current. Physical regularities of water exchange between the North Atlantic and the Arctic Ocean in 1958–2009 were analyzed on the basis of numerical experiments with eddy-permitting model of the ocean circulation with a resolution of 0.25° both along the longitude and latitude; they have shown that transversal oscillations of the Norwegian Current front were responsible for the formation of intermediate dense waters [11]. In this region, the zone of the vortex formation moving inside the LB has been noted [14, 15, 17].

A detailed review of the theoretical models by different authors describing the merging, regeneration, and stability of vortices is given in Bashmachnikov et al. [4].

In the introductory part of this contribution, the annual mean values of temperature, salinity, density, and ocean currents at the sea surface and depths up to 1500 m have been calculated for the whole region of the PS using the Argo model utilizing the Argo floats observations over the period 2005–2014. These observations showed the existence of the AV over the entire region of the LB with the

prevailing surface currents from 7–10 cm/s at the outer boundaries and up to 1–2 cm/s at the center of the LB; the current velocities decrease significantly with depth. At the same time, observations confirm the existence of a mesoscale lens at medium depths of 250–700 m over the deepest part of the LB. The evolution of the intratermocline lens, originally located in the central part of the LB depending on different types of velocity fields and the topographic effect are investigated using the contour dynamics method within the frames of the three-layer model.

## Observation Materials and Methods

Temperature and salinity data measured by the Argo floats covering the 10-year period from 2005 to 2014 [3] were used to study the hydrological structure and water dynamics in the LB. The studied area includes the North Atlantic (NA) and the Polar Seas (PS) of the Arctic Ocean (AO) from 55° to 80° N and from 30° W to 15° E. In this area about 17,600 temperature and salinity profiles from 125 Argo floats have been collected during 10 years of observations. In the LB area (68°–73° N and 5° W–12° E) there are 3273 profiles measured by 73 Argo floats. Seasonal mean data in addition to the 10-year annual mean fields were calculated in this region using 835 Argo profiles in winter, 679 in spring, 891 in summer, and 868 in autumn.

We used the AMIGO method ([10], see also http://argo.ocean.ru) for the data processing. Spatial resolution of data in the calculated database is one degree by longitude and latitude, the time resolution is one month. During the processing of the Argo profiles, we used the method of the variational interpolation of measurements onto a regular grid, followed by a model hydrodynamic adjustment of the fields. Such a procedure minimizes the errors when transferring irregularly located measurements into the regular grid; hence, the solution passes as close to the data as possible. At the final stage, using the ocean general circulation model in the diagnostic and hydrodynamic adjustment mode, we calculated the balanced monthly means and climatological temperature, salinity, density, and velocity fields based on the Argo data [10].

Taking into account that the one-degree calculation grid is rough for detecting and tracking the motion of mesoscale vortices with an average radius of about 37 km [15], we made an attempt to describe the structure and dynamics of the PS waters on the basis of the materials described above. The annual mean temperature, salinity, density, and flow velocity fields in this region were constructed at the depths from the sea-surface (associated with the 30 m level) to 1500 m depth. The maps and vertical sections of these characteristics in the central part of the LB, limited on the map by the isobath 3200 m, have clearly shown the existence of the AV at depths of 200–800 m. The vortex center is located at the point with coordinates 69.5° N, 3.5° E, which agrees with the results by Alekseev et al. [1], Ivanov and Korablev [6, 7], Köhl et al. [8], and Raj et al. [15].

Figure 2a shows a map of the annual mean velocity vectors in 1° squares at a depth of 30 m in the entire PS region. According to these data, two jets of the main transit currents are distinguished, transporting the warm and salty waters of the Atlantic Ocean to the AO. The eastern jet NwAC (Norwegian Atlantic Current) transports Atlantic waters from the area of the Faroe-Shetland Strait and follows along the Norway shore, round the Voring Plato from the east. Further, it flows to the north towards the Fram Strait, forming the Spitsbergen Current and a branch of the warm current in the Barents Sea. The western branch of NwAC enters the Norwegian Sea east of Iceland and flowing over the Norwegian Basin from the southeast, passes along the LB from the south and northwest, and then leaves the LB towards the Fram Strait. The Norwegian Coastal Current (NCC) is also clearly pronounced. This scheme of the location of the main jets completely coincides with the studies by Orvik and Niiler [13], Köhl et al. [8], Raj et al. [15], Rossby et al. [18], and Volkov et al. [24].

The maps in Fig. 2 show the current behavior in each layer of the model considered below: surface layer 0–255 m, intermediate layer 255–650 m, and deep layer up to 3000 m. The current velocity in the deepest layer is shown in the two lower panels.

Let us consider in detail the nature of the velocity field in the region adjacent to the LB. A large-scale anticyclonic vortex is observed in the water column from the surface and up to 1500 m above the entire area of the basin, shown on the map

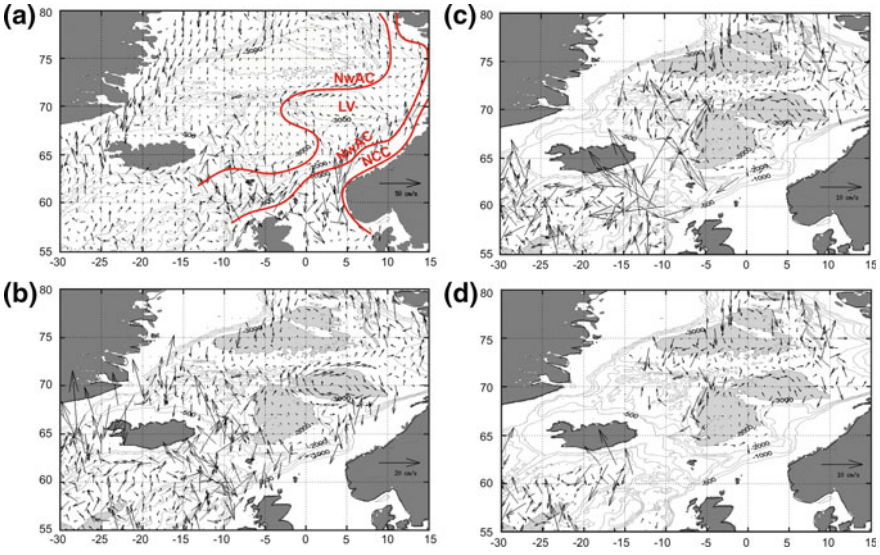


**Fig. 2** Annual mean velocity vectors in 1° squares of the AMIGO model at depths: **a** 30 m, **b** 400 m, **c** 1000 m, and **d** 1500 m. On panel (**a**), the jets of the main transit currents are marked by red lines, namely: eastern and western jets of the NwAC (Norwegian Atlantic Current) and the jet of NCC (Norwegian Coastal Current). The scales of the velocity vectors are different on different maps

within the isobath of 3000 m. Note that the western and northern parts of this vortex are formed by the western NwAC jet. In the northern part, there are two currents: a jet of the Atlantic waters directed northward and confined to the Mona Ridge, as well as a jet along the edge of the LB, which weakens when moving eastward. The structure of the AV in the LB is asymmetric: the velocities at its northern periphery at the 30 m level are 6–12 cm/s, 4–7 cm/s at 400 m, and 1–3 cm/s at 1000 m; the velocities at its southern periphery are 3–6 cm/s, 3–5 cm/s, and 0–1 cm/s, respectively, and in the center they range from 1–2 cm/s to zero. This means that a circular current exists in the 0–1500 m layer along the perimeter of the isobath 3000 m, which is better pronounced in its northern part. The velocities are weak (0–1 cm/s) in its central part. This current is located within the boundaries of the isobath 3200 m. Therefore, after analyzing these materials, it is possible to assume that an intrathermocline lens exists at the depths of 250–700 m within the LB with an average long-term position of its center at 69.5° N, 3.5° E. The lens forced by the topographic beta-effect drifts along a cyclonic trajectory. A similar result, according to the hydrological observations, was obtained by Alekseev et al. [1], in which the authors proposed to consider the scales of 60 and 130 km for describing the AV and LB.

Although the Argo observations give us a clear pattern of currents in the LB as part of the general circulation in the PS, they cannot serve as a basis for explaining the mechanisms of formation and displacement of vortices. In this relation, it is extremely important to conduct model studies within the framework of an adequate mathematical model, using estimates of the natural space and time scales. Below, we investigate the evolution of an intrathermocline lens in the central part of LB for different types of current fields using the three-layer version of the Contour Dynamics Method.

## Numerical Model and Simulation

Let us consider a model basin to explain the mechanism of the impact of the underwater depression on the behavior of the anticyclonic intrathermocline lens. We model the motion in the form of a set of two circular cylinders with displaced centers and with vertical walls which coincide with the 3000 and 3200 m isobaths.

Let the outer circle radius be equal to 132 km and the internal to 60 km; the height difference on each circle is 200 m, and their centers are in coordinates $(X_1;\ Y_1)$ and $(X_2;\ Y_2)$, respectively. We will use a quasi-geostrophic three-layer ocean model [20] with a piecewise-constant densities of $\rho_1, \rho_2, \rho_3$ between 0–250 m, 250–655 m, and 655–3000 m, respectively, and $\Delta\rho_1 = \rho_2 - \rho_1 = 0.00018\ \mathrm{g\,cm^{-3}}$, $\Delta\rho_2 = \rho_3 - \rho_2 = 0.00015\ \mathrm{g\,cm^{-3}}$. These values are typical for this water basin [4]. We assume that the vertical and horizontal scales are H = 3 km and L = 40 km, respectively; for the dimensionless layer thicknesses and radii of cylinders we get $h_1 = 0.0833$, $h_2 = 0.1383$, $h_3 = 0.7784$, and $R_1 = 3.3$, $R_2 = 1.5$.

We will also assume that the unperturbed external field consists of a combination of a homogeneous flow with horizontal velocities $U$, $V$, and a large-scale quasistationary anticyclonic vortex with characteristic azimuthal velocity $A$.

Taking into account the above assumptions, one can write the analytical expressions for stream functions $\psi_i$ of the horizontal motion in the layers [20, 21]:

$$\psi_i(x, y) = -Uy + Vx + A\left(x^2 + y^2\right) - \sum_{j=1}^{2} \sigma_j T_{ji}, \quad i = 1, 2, 3; \tag{1}$$

where

$$T_{ji} = \begin{cases} \frac{r_j}{4} - \frac{q_{i2}s_{23}}{s_{13}\gamma_1^2}\left[1 - \gamma_1 \mathrm{K}_1\left(\gamma_1 R_j\right)\mathrm{I}_0\left(\gamma_1 r_j\right)\right] - \frac{q_{i3}s_{33}}{s_{13}\gamma_2^2}\left[1 - \gamma_2 \mathrm{K}_1\left(\gamma_2 R_j\right)\mathrm{I}_0\left(\gamma_2 r_j\right)\right], & r_j \le R_j, \\ \frac{1 + \ln(r_j)^2}{4} - \frac{q_{i2}s_{23}}{s_{13}\gamma_1}\mathrm{I}_1\left(\gamma_1 R_j\right)\mathrm{K}_0\left(\gamma_1 r_j\right) - \frac{q_{i2}s_{23}}{s_{13}\gamma_2}\mathrm{I}_1\left(\gamma_2 R_j\right)\mathrm{K}_0\left(\gamma_2 r_j\right), & r_j \ge R_j, \end{cases}$$
$$j = 1, 2; \quad i = 1, 2, 3.$$

Here, index $i$ is the number of the layers (from top to bottom), and index $j$ is the cylinder number; $\sigma_j$ is an oriented height (negative for the depression) normalized by the horizontal section square of each of the cylinders, $r_j = \sqrt{\left(x - X_j\right)^2 + \left(y - Y_j\right)^2}$, where $x$ and $y$ are the coordinates of the observation point along the axes of the Cartesian coordinate system directed to the east and north respectively; $I_n$, $K_n$ $(n = 0, 1)$ are modified Bessel functions of the n order; $q_{ji}$ and $s_{ji}$ are the matrix elements.

$$Q = \begin{pmatrix} 1 & \frac{h_3\lambda_2}{\lambda_2 - \lambda_1} & -\frac{F_1}{h_1\lambda_2} \\ 1 & \frac{1}{\lambda_2 - \lambda_1}\left(h_2\lambda_2 + \frac{F_2}{h_2}\right) & -\left(\frac{F_1}{h_1\lambda_2} + 1\right) \\ 1 & \frac{1}{\lambda_2 - \lambda_1}\left[h_2\lambda_2 + \frac{F_2}{h_2} + \lambda_1 + \frac{F_1(h_1 + h_2)}{h_1 h_2}\right] & -\left[\frac{F_1}{h_1\lambda_2} + 1 + \frac{h_2}{F_2}\left(\lambda_2 + \frac{F_1(h_1 + h_2)}{h_1 h_2}\right)\right] \end{pmatrix}$$

and

$$S = Q^{-1} = \begin{pmatrix} h_1 & h_2 & h_3 \\ -\frac{h_2}{F_2}\left[\lambda_2 + \frac{F_1(h_1 + h_2)}{h_1 h_2}\right] & \frac{h_2}{F_2}\left[\lambda_2 + \frac{F_1(h_1 + h_2) + F_2 h_1}{h_1 h_2}\right] & -1 \\ -\frac{1}{\lambda_2 - \lambda_1}\left[\lambda_1 + \frac{F_1(h_1 + h_2)}{h_1 h_2}\right] & \frac{1}{\lambda_2 - \lambda_1}\left[\lambda_1 + \frac{F_1(h_1 + h_2) + F_2 h_1}{h_1 h_2}\right] & -\frac{1}{\lambda_2 - \lambda_1}\frac{F_2}{h_2} \end{pmatrix}.$$

Here, $\lambda_{2,1} = -\frac{1}{2}\left[\frac{F_1}{h_1} + \frac{F_1 + F_2}{h_2} + \frac{F_2}{h_3} \pm \sqrt{\left(\frac{F_1}{h_1} + \frac{F_1 + F_2}{h_2} + \frac{F_2}{h_3}\right)^2 - 4\frac{F_1 F_2}{h_1 h_2 h_3}}\right]$; $F_1 = (fL)^2/g_1' H$ and $F_2 = (fL)^2/g_2' H$ are Froude numbers $(g_1' = g\Delta\rho_1/\rho_0$, $g_2' = g\Delta\rho_2/\rho_0)$; $f$ is the constant Coriolis parameter, $g$ is the acceleration of gravity, $\rho_0$ is the mean density value.

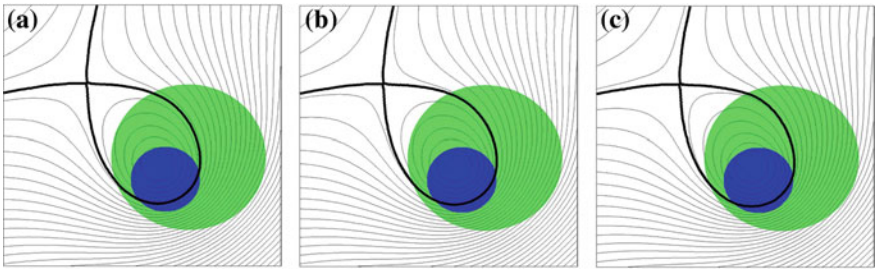


**Fig. 3** Phase portraits are shown as thin black lines for the barotropic external flow [1] over a cylindrical stepwise depression when $U = V = 10$ cm/s and $A = 0$. The section of the external cylinder is green, and the internal cylinder section is blue. Thick lines show separatices, which divide the areas of capture (with closed trajectories) and the areas with running flows of two types on the opposite sides of separatrices. Panels **a**, **b**, **c** are related to the upper, middle and lower layers, respectively

Figure 3 shows examples of fields $\psi_i$ when $(X_1;\ Y_1) = (0;\ 0)$ and $(X_2;\ Y_2) = (-1.5;\ -1.5)$. Panels "**a**", "**b**", "**c**" represent phase portraits in the upper, middle and lower layers, respectively, in the particular case $A = 0$ when the depression is surrounded by the barotropic northeast stream. Cyclonic relative vorticity is generated owing to the conservation of the potential vortex in the vicinity of the depression [9]. Even at a considerable distance from the depression the flow remarkably twists counterclockwise, and a quasi-barotropic topographic cyclone with a small predominance of capture in the lower layer is formed in the western part of the depression.

Figure 4 depicts stream function $\psi_2$ in the middle layer, in the case $A < 0$. Panels **a–d** demonstrate the effect of an external anticyclonic vortex on the field function behavior of horizontal velocities. Here, four phase portraits are given for the case of the current type [1] and $A = -0.005,\ -0.01,\ -0.02\ -0.04$, which correspond to the azimuthal velocity values $v = -0.9,\ -1.8,\ -3.6,\ 7.2\,\mathrm{cm\,s^{-1}}$ on the circular isobath 3000 m. It can be seen that the presence of an external large-scale anticyclone, contributes to the reduction of the area of the cyclonic Taylor column until it disappears completely (panel "**d**"), when it fills the space above the depression almost completely suppressing the topographic effect. At moderate values of the

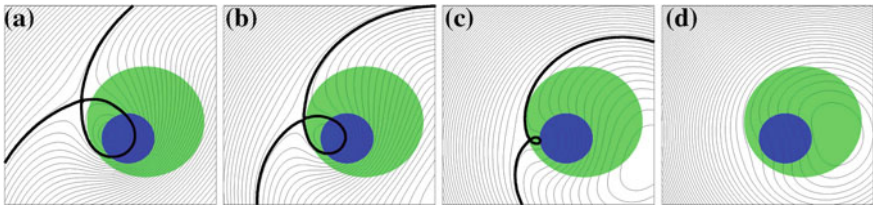


**Fig. 4** The same as in Fig. 3, but for the middle layer: **a** $A = -0.005$, **b** $A = -0.01$, **c** $A = -0.02$, **d** $A = -0.04$

intensity of the anticyclone (panels "**a**" and "**b**"), one can speak about the qualitative agreement with Fig. 2, identifying the bundle of isolines, located to the right from the separatrix loop, with the eastern stream NwAC, and the one to the left with the west side. The same can be said about the phase portraits in Fig. 3.

The resulting velocity distributions will now be used as "external fields" for the anticyclonic lens, localized in the pycnocline [6, 7, 23]. Hereinafter, we will consider processes that take place only in the corresponding middle layer.

Without resting on the problem of the anticyclonic lens in the vicinity of a topographic vortex (these questions are discussed in detail in Ivanov and Korablev [6, 7]), we consider several versions of the different behavior of the lens depending on its initial location.

Let us consider separately cases (I) without taking into account the vortex ($A = 0$), and (II) taking into account the effect of anticyclonic rotation on the external flow ($A < 0$).

**Case (I)**. At the initial time moment, we assume that the lens has a circular shape with dimensionless radius $r_{lens} = 0.6$, which corresponds to 60 km, and represents a vortex patch belonging to the middle layer, which is a region with a constant value of potential vorticity (PV). In this case, the initial PV value determines the time scale. Assuming the azimuthal velocity at the outer edge of the lens to be 20 cm/s, we will choose PV such that the rotation period of its liquid particles is equal to 20 days. This period will correspond to a unit of dimensionless time in numerical experiments.

In the presence of a lens, the phase portrait is constructed taking into account its effect on the current function field using the Contour Dynamics Method developed for the three-layer rotating liquid [20].

In the first experiment, shown in Fig. 5, the initial position of the lens center coincides with the stationary elliptic point inside the cyclonic topographic vortex, which is located inside the separatrix loop of the current function for the middle

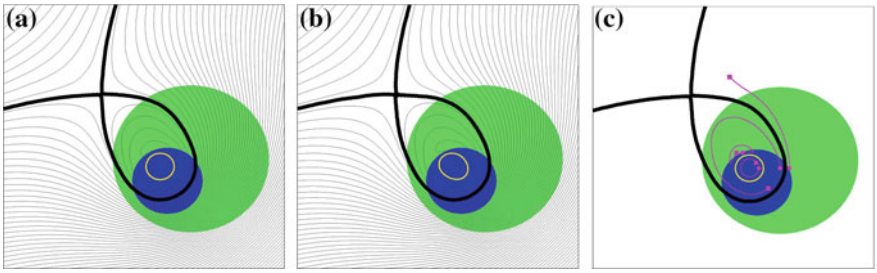


**Fig. 5** Stream function field of the middle layer $\psi_2$ in the vicinity of the submerged depression in the case of the lens presence. The center of the lens is located at a "motionless" point of the separatrix loop in "**a**" and "**b**" panels (a 20-day interval corresponds to the unit of dimensionless time). Panel "**c**" shows the initial parts of the trajectory of fluid particles, placed both inside the lens and at its vicinity. In all panels, a thick yellow line represents the lens contour. Trajectories of fluid particles and markers (round as the initial position, and square as the last calculated position) are shown in by magenta color in panel "**c**"

layer. Assuming the selected external parameters, this point has coordinates (−1.3098; −0.3511). Panel "**a**" shows that, in this case, the lens does not virtually affect the kinematic characteristics of the flow outside the topographic vortex. Changes are observed only in the inner part of the separatrix loop. Panel "**b**" shows that the position of the lens can be considered almost quasistationary. Indeed, when $t = 10$, i.e., more than 6 months after the beginning of motion, the lens center remains in its initial position. Of course, the lens does not retain a circular shape, since the external field is not axisymmetric, but the position of its center stably holds almost the same place. Panel "**c**" shows the behavior of several liquid particles inside and outside the lens. Three of the four selected material points are initially located at the latitude of the lens center and move as follows: (1) the particle inside the lens rotates along a closed circular path in the anticyclonic direction, (2) the particle between the lens and the boundary of the separatrix loop rotates along the cyclonic path, remaining inside the topographic cyclone, (3) the particle located outside the separatrix loop is carried away by the current beyond the depression. Finally, the particle, initially located north of the lens boundary, moves along a hole-shaped path reminding the configuration of the corresponding isoline of the current function.

This experiment suggests that the region of the capture of an anticyclonic lens by a cyclonic topographic vortex cannot only be confined to a motionless elliptic point but may have finite dimensions.

The next series of calculations presented in Fig. 6, confirms and concretizes the latter assumption. In this figure, the lenses themselves are not shown; it gives only the trajectories of their centers. In panel "**a**", at the initial time, this center is placed at the hyperbolic point of the separatrix of the current function field with coordinates (−4.4001, 3.3899). Theoretically, this singular point is the place of attraction of the trajectories, and the calculation does, in fact, show that the center of the lens remains in place for quite a long time. But since the coordinates of the hyperbolic point are calculated approximately, then, because of the instability of the equilibrium position, the lens begins to move along a trajectory passing in a very close neighborhood of the separatrix. After a nearly complete tour along the loop, the lens is again slowing down in the vicinity of the hyperbolic point, but then it breaks off

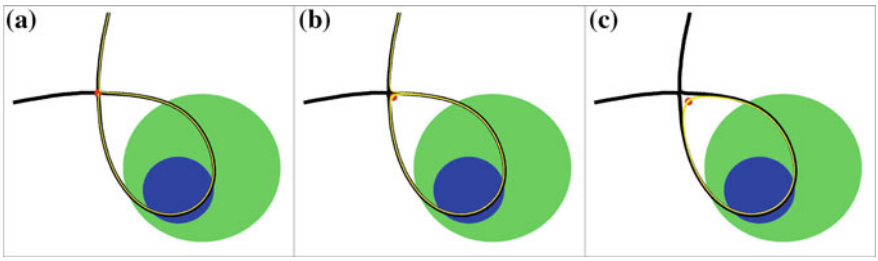


**Fig. 6** Trajectories (yellow lines) of the lenses' centers are initially localized in the hyperbolic point of the unperturbed separatrix and in its vicinity. Red markers depict initial positions of the lenses' centers: (−4.4001; 3.3899) in panel "**a**"; (−4.2; 3.2) in panel "**b**"; (−4.0; 3.0) in panel "**c**"

from the closed part of the trajectory and is carried away by a stream along one of the separatrix "whiskers".

A small displacement of the initial position of the lens center inside the separatrix loop (Fig. 6b, where the initial coordinates of the center are indicated in the caption) leads to the fact that now the lens makes three revolutions inside the loop along an insignificantly untwisting spiral, and then, like the previous case, is carried away by flow beyond the depression. Finally, if the displacement of the initial position of the lens center toward the center of the topographic vortex becomes larger (Fig. 6c), the lens is completely captured by the topography. At the end of the calculation time interval, the lens performed 10 complete cycles. This series of calculations shows that the region of the lens capture by the depression occupies almost the entire separatrix loop of the current function except for a small neighborhood near the hyperbolic singular point. It is important to note that the capture can take place even in the case when the lens is originally located outside the depression (the figure in panel "**c**" shows this clearly). Thus, the trajectory of the lens center in panel "**c**" can be approximately taken as the outer contour of the cross section (in the middle layer) of the Taylor column [7, 9, 25], which limits the region of the initial positions of the lens centers that do not leave the vicinity of the depression.

The unperturbed separatrix of the phase portrait of the middle layer is shown in all three panels of Fig. 6. However, it is obvious that the presence of a lens (if it is not initially placed at a stationary elliptic point, as in Fig. 5) substantially alters the entire structure of the flow and the configuration of the separatrices in particular.

Figure 7 shows how a lens affected by an "external field" changes the field of the current function over the depression and at its vicinity. Here, we show a sequence of instantaneous lens configurations in the case presented in Fig. 6a, when, at the initial moment, the lens center was located at the hyperbolic point of the unperturbed separatrix. In all panels, the stationary unperturbed separatrix is depicted by a grey solid line. It is not related to the real non-stationary velocity field and is only a marker curve that tracks the motion of the lens center. The first panel shows that already at $t = 0$, two separatrices begin their formation (red and black solid lines) in the current function field. Note that, theoretically, at this stationary point they should merge, but as mentioned above, the coordinates of the hyperbolic point are calculated with an error, and therefore two separatrices have a small relative displacement (the black line has a self-intersection point located to the southwest of the lens center, and red one to the northeast). This experiment also gives an opportunity to demonstrate the uneven motion of the lens along its trajectory. Indeed, since the starting position is connected with a stationary point of the phase portrait, at the initial stage of the movement, the lens moves very slowly (the second panel corresponds to time $t = 8$). Then the motion accelerates, and the maximum velocity of the lens along the trajectory occurs at the maximum distance from the initial position. In the course of the lens re-approach to the hyperbolic point of the unperturbed separatrix, its motion slows down again (see indicated times at the panels). Note that a similar effect appeared in the calculations by Köhl et al. [8] (see Fig. 11).

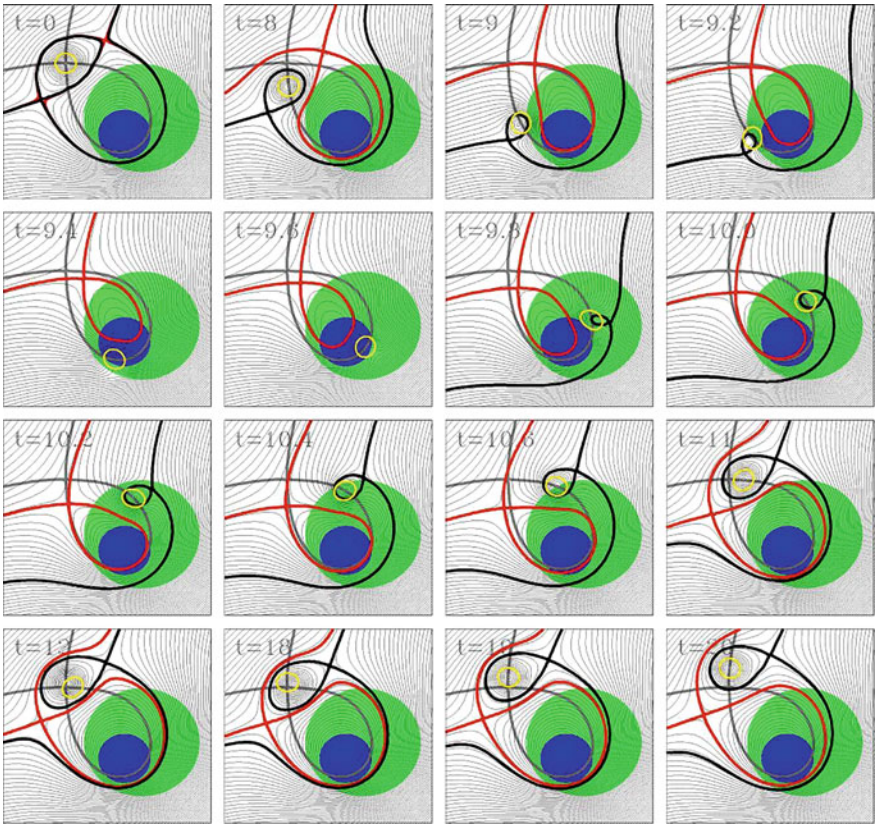


**Fig. 7** Time scans of the sequence of the lens instantaneous positions at its initial location at the hyperbolic point of the unperturbed separatrix (gray solid lines) at the indicated moments of the dimensionless time. Two separatrices are forming in the field of the current function represented by black and red solid lines

It is easy to see that at each time moment the black separatrix loop is associated with the local position of the lens, and the red separatrix loop is associated with the bottom relief. It should be noted that the first of them decreases (and even disappears in the interval 9.2–9.4) in the vicinity of the maximum velocities of the lens motion. This can be explained by the weakening of the local anticyclonic swirl of the flow due to the increased influence of the topographic cyclone. The demonstration of the controlling role of the unperturbed separatrix during all stages of the lens motion, despite the complex nature of the evolving field of horizontal velocities is an important result of this and previous experiments.

**Case (II)**. Let now the external flow, in addition, have a general anticyclonic rotation ($A < 0$).

Figure 8 shows the behavior of the captured lens against the background of instant phase portraits at $A = -0.01$. In this case, the hyperbolic self-intersection

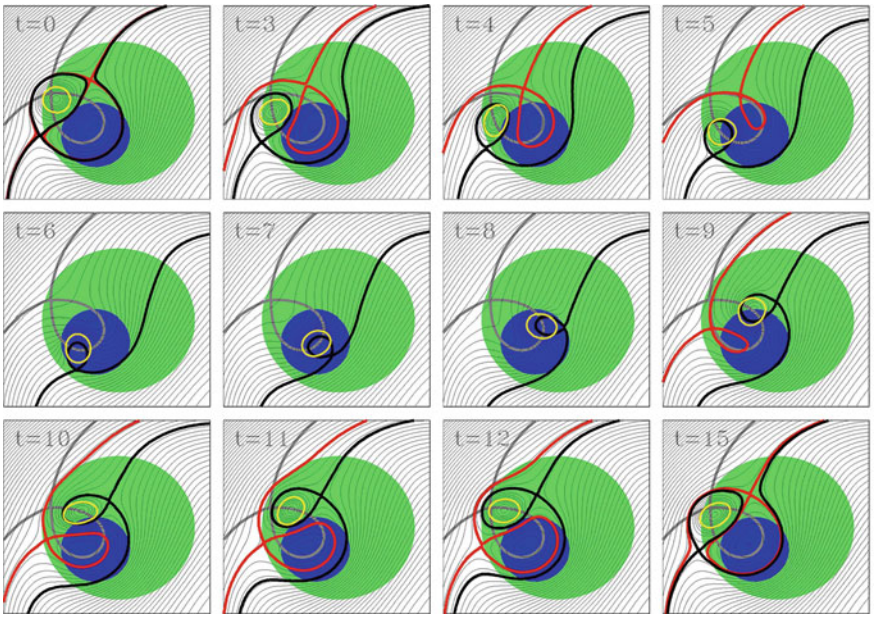


**Fig. 8** The same as in Fig. 7, but taking into account a large-scale anticyclonic vortex in the local area of the depression at $v = -1.8\,\mathrm{cm\,s^{-1}}$, in the case when the initial position of the lens is located inside the loop of the unperturbed separatrix in the vicinity of the hyperbolic point

point of the separatrix has coordinates (−2.899, 0.905), and the initial position of the lens center is inside the loop at the point (−2.70, 0.63). It is seen that under such conditions the lens remains trapped, and its center describes a closed trajectory inside the separatrix loop. This figure shows the calculations results over an interval, slightly longer than one period. As in the experiment shown in Fig. 7, the rotation is not uniform: it slows down along the trajectory near the hyperbolic singular point and accelerates in the course of motion away from this point along the trajectory. The most significant changes in the volume of the loop are observed on the red separatrix associated with the bottom relief. It decreases, and can even completely disappear (moments 60, 70, and 80), when the anticyclonic lens passes over the deepest part of the basin and, thus, partially neutralizes the cyclonic twist induced by the depression that prevents the formation of a region of closed trajectories.

We note an interesting side effect: a periodic occurrence of a meandering jet at time intervals when the black and red separatrices are separated by a specific distance (intervals 3–5 and 9–12). For example, at $t = 12$, fluid particles in this stream, located between the "whiskers" of the black and red separatrices, approach the depression from the southwest; over the depression, they round one of the loops, pass between two loops, round the second loop, and finally leave the vicinity of the depression in the northeastern direction. When the separatrices are close to each

other ($t = 0$ and $t = 15$), the jet vanishes, and the flow rounds the region of the hugged loops, like one solid body.

Figures 4 and 8 show that, despite the external anticyclonic rotation, a cyclonic Taylor column can be formed over the depression during a specific interval of the anticyclone intensity. This column is capable to capture and twist counter-clockwise passive liquid particles as well as vortices inside it. This gives an explanation to the seemingly strange cyclonic direction of the observed lens motion in the works by Ivanov and Korablev [6, 7]. In the case where the initial location of the lens center is outside the Taylor column, the lens leaves the vicinity of the LB.

## Conclusions

The formation, drift, and destruction of mesoscale vortices within the LB occur against a background of the large-scale processes in the study site. Hence, the PS is a buffer zone of the water exchange between the North Atlantic and the Arctic Ocean [11]. The complex character of their interaction determines the seasonal and multi-year variability of the hydrological regime and dynamics of the PS and, in particular, the LB. Raj et al. [15] note the inter-annual and seasonal variability of the number of observed vortices in the investigated basin and their relationship to these external processes. It should be kept in mind that it is almost impossible to recreate in the model experiment the complete similarity with the real ocean conditions. However, such modeling, in spite of some assumptions, allows us to trace all the stages of the influence of the external parameters on the behavior of the intrathermocline lens. In this contribution based on the results of various experimental observations, the existence of a quasi-permanent intratermocline lens in the vicinity of the deep part of the LB is postulated as a fact. Within the framework of the numerical model, we model various scenarios of the lens motion, which can take place in the ocean. In particular, it is clearly shown that (1) the lens not captured by the quasi-stationary Taylor column leaves the LB region, (2) the lens located in the vicinity of the hyperbolic point can remain for a long time in the quasistatic state, (3) the lens belonging to the inner part of the Taylor column, which is associated with the separatrix loop of the stream function, performs closed periodic rotations in the cyclonic direction. The latter can occur even in presence of a large-scale anticyclonic vortex of moderate intensity. The model conclusions about the behavior of the quasi-constant anticyclonic vortex in the LB coincide with the main observed results. They also give an idea of the physical processes that determine the various conditions of its cyclonic drift depending on the variability of the velocity field characteristics and the topographic effect.

**Acknowledgements** The work was supported by Russian Science Foundation (grant 14-50-00095) (analysis of the ocean data) and Ministry of Education and Science of the Russian Federation (grant 14.W03.31.0006, (numerical simulation), and Russian Foundation of Basic Research (grant 16-55-150001) (vortex dynamics).

## References


1. Alekseev, G. V., Bagryantsev, M. V., Bogorodskiy, P. V., Vasin, V. V., & Shirokov, P. E. (1991). Structure and circulation of water in the area of anticyclonic eddy in the northeastern Norwegian Sea. *Problems of the Arctic and Antarctic, 65,* 14–23 (in Russian).
2. Alekseev, G. V., Nikolaev, Yu V, Romanov, A. A., Romantsev, V. A., & Sarukhanyan, E. I. (1986). Results of natural investigations in the Norwegian energy active zone. *Itogi Nauki i Tekhniki, Atmosphere, Ocean, Space Program RAZREZY, 7,* 46–72 (in Russian).
3. Argo. (2000). Argo float data and metadata from Global Data Assembly Center (Argo GDAC). SEANOE. http://doi.org/10.17882/42182.
4. Bashmachnikov, I. L., Sokolovskiy, M. A., Belonenko, T. V., Volkov, D. L., Isachsen, P. E., & Carton, X. (2017). On the vertical structure and stability of the Lofoten vortex in the Norwegian Sea. *Deep-Sea Research Part I* (in press).
5. Gascard, J.-C., & Mork, K. A. (2008). Climatic importance of large-scale and mesoscale circulation in the Lofoten Basin deduced from Lagrangian observations. In R. R. Dickson, J. Meincke, & P. Rhines (Eds.), *Chapter 6: Arctic-Subarctic Ocean fluxes. Defining the role of the Northern Seas in climate* (pp. 131–143). Dordrecht: Springer.
6. Ivanov, V. V., & Korablev, A. A. (1995). Formation and regeneration of the pycnocline lens in the Norwegian Sea. *Russian Meteorology and Hydrology, 9,* 62–69.
7. Ivanov, V. V., & Korablev, A. A. (1995). Interpycnocline lens dynamics in the Norwegian Sea. *Russian Meteorology and Hydrology, 10,* 32–37.
8. Köhl, A. (2007). Generation and stability of a quasi-permanent vortex in the Lofoten Basin. *Journal of Physical Oceanography, 37,* 2637–2651.
9. Kozlov, V. F. (1984). *Models of the topographic vortices in ocean* (p. 200). Moscow: Nauka.
10. Lebedev, K. V. (2016). An argo-based model for investigation of the Global Ocean (AMIGO). *Oceanology, 56,* 172–181.
11. Moshonkin, S. N., Bagno, A. V., Gusev, A. V., Filyushkin, B. N., & Zalesny, V. B. (2017). Physical properties of the Atlantic-Arctic water exchange formation. *Izvestiya Atmospheric and Oceanic Physics, 53,* 213–223.
12. Orvik, K. A. (2004). The deepening of the Atlantic water in the Lofoten Basin of the Norwegian Sea, demonstrated by using an active reduced gravity model. *Geophysical Research Letters, 31,* L01306. https://doi.org/10.1029/2003GL018687.
13. Orvik, K. A., & Niiler, P. (2002). Major pathways of Atlantic water in the northern North Atlantic and Nordic Seas toward Arctic. *Geophysical Research Letters, 29*. https://doi.org/10.1029/2002GL015002.
14. Poulain, P.-M., Warn-Varnas, A., & Niiler, P. P. (1996). Near-surface circulation of the Nordic Seas as measured by Lagrangian drifters. *Journal Geophysical Research, 101,* 18237–18258.
15. Raj, R. P., Chafik, L., Nilsen, J. E. Ø., Eldevik, T., & Halo, I. (2015). The Lofoten Vortex of the Nordic Seas. *Deep-Sea Research Part I, 96,* 1–14.
16. Raj, R. P., & Halo, I. (2016). Monitoring the mesoscale eddies of the Lofoten Basin: Importance, progress, and challenges. *International Journal of Remote Sensing, 37,* 3712–3728.
17. Rodionov, V. B., & Kostianoy, A. G. (1998). *Oceanic fronts of the North-European basin seas* (293 pp.). Moscow: GEOS (in Russian).
18. Rossby, T., Ozhigin, V., Ivshin, V., & Bacon, Sh. (2009). An isopycnal view of the Nordic Seas hydrography with focus on properties of the Lofoten Basin. *Deep-Sea Research Part I, 56,* 1955–1971.
19. Søiland, H., & Rossby, T. (2013). On the structure of the Lofoten Basin Eddy. *Journal of Geophysical Research: Oceans, 118,* 4201–4212.
20. Sokolovskiy, M. A. (1991). Modeling triple-layer vortical motions in the ocean by the Contour Dynamics Method. *Izvestiya Atmospheric and Oceanic Physics, 27,* 380–388.

21. Sokolovskiy, M. A., & Verron, J. (2014). Dynamics of vortex structures in a stratified rotating fluid. In *Series Atmospheric and oceanographic sciences library* (Vol. 47, p. 382). Switzerland: Springer International Publishing.
22. Voet, G., Quadfasel, D., Mork, K. A., & Søiland, H. (2010). The mid-depth circulation of the Nordic Seas derived from profiling float observations. *Tellus, 62A,* 516–529.
23. Volkov, D. L., Belonenko, T. V., & Foux, V. R. (2013). Puzzling over the dynamics of the Lofoten Basin—A sub-Arctic hot spot of ocean variavility. *Geophysical Reseach Letters, 40,* 738–743.
24. Volkov, D. L., Kubryakov, A. A., & Lumpkin, R. (2015). Formation and variability of the Lofoten Basin vortex in a high-resolution ocean model. *Deep-Sea Research Part I, 105,* 142–157.
25. Zyryanov, V. N. (1995). *Topographic eddies in sea currents dynamics* (p. 240). Moscow: Water Problems Institute of RAS (in Russian).